The Journal of Chemical Physics

Absolute ionization and dissociation cross sections of tetrahydrofuran: Fragmentation-ion production mechanisms

Cite as: J. Chem. Phys. **151**, 064304 (2019); https://doi.org/10.1063/1.5115403
Submitted: 17 June 2019 . Accepted: 19 July 2019 . Published Online: 09 August 2019

W. Wolff, B. Rudek, L. A. da Silva, G. Hilgers, E. C. Montenegro, and M. G. P. Homem

The Journal of Chemical Physics ARTICLE scitation.org/journal/jcp

Absolute ionization and dissociation cross sections of tetrahydrofuran: Fragmentation-ion production mechanisms

Cite as: J. Chem. Phys. 151, 064304 (2019); doi: 10.1063/1.5115403
Submitted: 17 June 2019 • Accepted: 19 July 2019 •
Published Online: 9 August 2019

W. Wolff,[1,a] B. Rudek,[2] L. A. da Silva,[3,b] G. Hilgers,[2] E. C. Montenegro,[1] and M. G. P. Homem[3]

AFFILIATIONS

[1]Instituto de Física, Universidade Federal do Rio de Janeiro, 21941-972, Rio de Janeiro, RJ, Brazil
[2]Physikalisch-Technische Bundesanstalt, Bundesallee 100, Braunschweig, Germany
[3]Departamento de Química, Universidade Federal de São Carlos, 13565-905, São Carlos, SP, Brazil

[a]**Electronic mail:** wania@if.ufrj.br
[b]**Present address:** Instituto de Química de Araraquara, Universidade Estadual Paulista Júlio de Mesquita Filho, 14800-901, Araraquara, SP, Brazil.

ABSTRACT

We report an experimental and theoretical investigation on the absolute ionization and fragmentation cross sections of tetrahydrofuran (THF, C_4H_8O), a base molecule of the DNA-backbone. The measurements enabled the identification of 50 ionic species produced by 12 eV up to 2000 eV electron impact which allowed us to make a close inspection of the mechanisms of both the primary vacancy production and the postcollisional fragmentation pathways which lead to the fragment ions. The experimental cross sections of the ionic species were examined in the framework of the fragmentation matrix model to attribute from which molecular orbitals (MOs) the electron is removed and find out the relative contribution of up to 15 outer and inner valence MOs in the fragment-ion production. A comparison between measured and calculated dissociative cross sections relative to the molecular parent ion cross section allowed us to clearly identify the prevalence of the single or double ionization in the fragment-ion production. Due to these different production mechanisms, the relative proportion of some ejected fragment-ions strongly depends on the impact energy. The single ionization of the MOs leading to selected fragment ions was compared to those measured at a low electron-impact energy using a reaction microscope with good agreement between the two techniques. The formation of the dications $C_4H_nO^{2+}$, excluding the molecular parent dication, is also presented.

I. INTRODUCTION

Radiation damage in cells is based on the interaction of ionizing radiation with molecular building blocks of the genome. Describing the ionization and fragmentation in biological systems thus requires studies on the impact of charged particles on deoxyribonucleic acid (DNA) and ribonucleic acid (RNA).[1] Electrons penetrating biological media induce damage in these structures, in particular, by breaking the strands of the nucleic acids.[2] Deoxyribose and ribose in DNA and RNA, respectively, are pentose sugars, and the tetrahydrofuran molecule (THF) is regarded as the prototype for the structural unit of these sugar moieties.[3] In a simple model of the DNA, a series of THF molecules are bound to phosphate units and the base analogs pyrimidine or purine.[4] In the pharma-biological context, derivatives of THF also form important anti-HIV (Human Immunodeficiency Virus) and anti-AIDS (Acquired Immune Deficiency Syndrome) drugs.[5]

Several experimental as well as theoretical studies are available on THF interaction cross sections covering elastic,[6–18] inelastic,[14–16,19–21] excitation,[15,19–21] and integral electron impact cross

sections.[4,7,14,15,19–25] On the theoretical side, several semiempirical and semiclassical models have been developed with most of them based on the additivity theorem, according to which the molecular cross sections are determined as a sum of contributions from atomic orbitals specified by the Mulliken population.[26,27] Other theoretical models also provided ionization cross sections.[4,15,16,21,23,24,26,27]

For electron-impact ionization of THF, five measurements of the absolute total ionization are available in the literature to the best of the authors' knowledge, but the absolute partial dissociative cross sections (PDCSs) are rather sparse. For the fragmentation of THF, Dampc *et al.*[28] reported measurements for electron impact energies from 20 eV to 140 eV and Fuss *et al.*[20] within 50 eV–5000 eV electron energy range. The data of Dampc *et al.* cover the electron energy region of the total ionization cross section (TICS) maximum and include the absolute PDCSs of nine ionic fragment species, while the measurements of Fuss *et al.* extend up to 5000 eV electrons reporting the PDCSs summed up in ion-groups of carbon atoms plus the oxygen atom. To complete the experimental data of electron-induced ionization of THF, we report here the absolute PDCSs of 43 singly charged fragment-ions, the absolute parent ionization cross sections (PICSs) of the molecular parent-ion and of two heavier ionic isotopes, and the identification of four dications within the 10 eV–2000 eV electron energy range filling the gap of the experimental data and giving a more comprehensive scenario of the fragmentation pattern.

Due to the present impracticability of theoretically treating the dissociation following ionization of polyatomic molecular species from first principles, we developed a semiempirical fragmentation model to associate the magnitude and shape of the fragment-ion cross sections with the single vacancies created in the molecular orbitals.[29,30] These studies were successfully carried out before for electrons and protons impacting on small molecules, such as water and methane,[30–33] as well as on larger organic molecules, such as pyrimidine and pyridazine.[29,34] The fragmentation matrix model (FMM) allows us to estimate the contribution of the single ionization from individual molecular orbitals to the production of each ionic fragment species and the quantification of the multiple ionization process in the ion-formation. The experimental signature of multiple ionization to the fragment ion production is given by the deviation of the measured fragment-ion cross sections. These cross sections are calculated by the fragmentation matrix model, which considers only the single ionization process as the transition pathway to fragmentation.

In Sec. II, the experimental technique and procedures are described. The results of our measurements are presented and discussed, and compared with available experimental and theoretical data in Sec. III. It is divided into the subsections for total ionization cross section, dissociative ionization cross section, fragmentation-ion production mechanisms, doubly charged fragment-ions, and fragmentation matrix. In Sec. IV, the results are summarized.

II. EXPERIMENTAL

The ionization and partial dissociation measurements were performed at the division of Ionizing Radiation of the Physikalisch—Technische Bundesanstalt (PTB) (Braunschweig, Germany) using an experimental setup which has been used before for electron-impact ionization experiments with hydrocarbons such as trimethylphosphate, pyrimidine, tetrahydrofuran, chlorobenzene, and pyridine.[35–37] Details of the setup and the measurement procedures have been provided previously, and a brief presentation is included here.

The setup is composed of a commercial pulsed electron gun (Kimball ELG-2), a reflectron time-of-flight mass spectrometer (Mini-TOF-MS by Kore Technologies, Ltd.), and a gas cell. The components were mounted as close as possible to another. A pair of Helmholtz coils was used for compensation of the Earth's magnetic field and to guide low-energy electrons axially. The electron beam of 100 ns pulse length, the beam current of around 80 nA, and the repetition rate of 50 kHz was collected by a Faraday cup after traversing the gas cell entrance and exit apertures of 4 mm in diameter. During the experiments, the beam current was monitored by a picoammeter and recorded by Labview software. The measurements were performed at electron energies between 10 eV and 2000 eV. The electron beam was monitored using a YAG-crystal screen placed close to the gas cell exit and with a Faraday cup with an entrance collimator. The two extraction electrodes of the mass spectrometer were enclosed within the gas cell, and an extraction pulse of 350 V and 1 μs in length was applied to the isolated extraction electrode to start the time-of-flight recording. The delay between the extraction pulse and the pulsed electron beam was set as short as possible not to lose fast fragments. The extracted ions were focused by an electrostatic lens, accelerated to 2 keV and deflected into an array of electrodes, where the applied voltage increases from −2 kV to 0 V to reflect the ions toward a discrete dynode electron multiplier detector (ETP AF824 by Scientific Instrument Services, Inc.). The detector gain was adjusted to give highest efficiency for large masses. The spectrometer chamber was differentially pumped to guarantee a high-vacuum environment for the detector at 1×10^{-8} mbar when the experimental chamber was operated with the sample gas at 1×10^{-6} mbar. An absolute capacitive manometer attached to the gas inlet monitored the gas pressure amounting to 0.007 mbar on average and was recorded by Labview software.

The absolute total ionization cross section (TICS) as a function of the electron energy from 20 to 1000 eV was obtained at Chemistry Department of the Federal University of São Carlos (UFSCar) using the relative flow technique (RFT).[38] The intensities of ions were measured using a crossed geometry of collimated electron and molecular beams. A pulsed and magnetically collimated electron gun produced a stable electron beam with 50 ns width and a repetition rate of 300 μs in the energy range of 1–1000 eV. The electron currents ranging around 50–150 pA with an energy resolution of about 0.5 eV full-width at half-maximum were monitored by a Faraday cup. The target gas was delivered through a set of microcapillaries with individual diameters (d) of 50 μm and 5 mm length (L), defining an aspect ratio (d/L) of 0.01. After the electron-molecule interaction, the ions were extracted toward a TOF-MS located perpendicularly to the plane of the electron beam and the target gas beam. The background pressure of the experimental chamber was around 1×10^{-7} mbar, and during the measurements, with sample admission, the typical pressure increased to $0.8–3 \times 10^{-6}$ mbar. The absolute pressure in the gas line was measured through a capacitive membrane manometer (624B01T MKS Baratron). The ions were extracted out of the collision region by a high-voltage extraction field, which ensured the collection of ions with energies up to 20 eV. An extraction potential of 150 V was applied

to a pair of wire meshes, symmetrically placed on the sides of the collision region. It was switched with a delay of 150 ns with respect to the pulsed electron beam. A Wiley-McLaren TOF spectrometer with the total drift length of 270 mm directed the ions toward a single electron multiplier (channeltron), and after signal processing, the ion intensities were analyzed by a time-to-digital converter (ID801-TDC by ID Quantique SA). The transmission efficiency of the spectrometer (including ion source, TOF-MS, and detector) was optimized with known ionization cross sections of rare gases (Ar and Xe).[39,40]

The recorded intensities are converted into absolute ionization cross sections using the RFT.[38,41] For a given impact energy (E), the intensity (I) of the ionic fragments per unit of incident electron beam current can be expressed as[41]

$$I(E) = \frac{\eta\,\sigma(E)}{v}\,\beta, \tag{1}$$

where σ refers to the ionization cross section, η is the efficiency of the detection system, v is the mean velocity of molecules in the gaseous beam, and β is related to the interaction volume defined by the intersection between the gas and the electron beam.[41] The latter is not trivially obtained since it depends on the collision geometry as well as some beam properties such as spatial and velocity distributions, which are difficult to be determined experimentally. The ratio of intensities measured for the gas under study (THF) and a secondary standard (*std*) are related to the corresponding cross sections as

$$\frac{I_{THF}}{I_{std}} = \frac{\sigma_{THF}}{\sigma_{std}}\,\frac{\beta_{THF}}{\beta_{std}}\,\sqrt{\frac{M_{THF}}{M_{std}}}, \tag{2}$$

where M is the molecular weight. If the beam profiles of the two gases are closely the same, then it can be shown[41] that

$$\frac{\beta_{std}}{\beta_{THF}} = \frac{R_{std}}{R_{THF}}, \tag{3}$$

where R is the relative flow rate. Therefore, the σ_{THF} for a gas under determination can be related to known σ_{std} of a secondary standard as

$$\sigma_{THF} = \sigma_{std}\,\frac{I_{THF}}{I_{std}}\,\frac{R_{std}}{R_{THF}}\,\sqrt{\frac{M_{std}}{M_{THF}}}. \tag{4}$$

Usually, this condition is achieved using the ratio of pressures that ensures the equal mean-free-path condition, that is, $P_{THF}/P_{std} = \delta_{std}^2/\delta_{THF}^2$, where δ is the molecular diameter.

When the mean-free path of the gas is comparable or fractionally less than the tube length, the flow rate R can be approximated as a second order polynomial dependent on the target backing pressures P,[42] $R = k_1P + k_2P^2$. Due to the high mass and polar nature of the THF, in the present work, the kinetic parameters k_1 and k_2 were determined following the procedure described in Ref. 42. This procedure is very useful in the determination of R for sticky species, overcoming the problem of the adsorption of the gases at surfaces. The same procedure was applied to the secondary standard N_2 and Xe.

The absolute values were obtained by applying the RFT to the parent ion ($C_4H_8O^+$) resulting in the parent ionization cross sections (PICSs), and the partial dissociative cross sections (PDCSs) for all other fragments were obtained from this value. For that, the intensities of the $C_4H_8O^+$ and the N_2^+ and Xe^+ were recorded at several equilibrium backing pressures P to verify a linear behavior between I and $R\sqrt{M}$ to apply Eq. (4). The N_2^+ and Xe^+ ionization cross sections reported by Straub *et al.*[43] and Rejoub *et al.*[40] were used. While this study may not have reached the molecular flow regime, this equation is still valid as the detector's field-of-view covered the entire collision region and the electron beam flux was uniform so that the ratio β/R was comparable for all gases.[41] Additional cross-checking tests were conducted using the equal mean-free-path condition.

The TICSs were obtained by summing up the PICSs and PDCSs. The statistical uncertainties from the peak areas were typically well below 2% over the entire energy range since almost no or little overlap between the mass peaks was present in the high-resolution TOF spectra of the PTB setup. The experimental uncertainties of the TICS obtained at UFSCar were determined as follows: uncertainties of random nature such as pressure fluctuations, electron beam current readings, and background contributions were estimated to be less than 2%. These contributions combined with the estimated statistical errors give an overall uncertainty of 4% in the relative measurements for each gas. Adding the reported uncertainties for the reference gases,[40,43] the estimated standard deviations in the TICS were 15%.

Tetrahydrofuran is liquid at room temperature. The liquid sample purchased from Sigma-Aldrich with purity greater than 99.8% was placed in a glass vial containing molecular sieves. It was degassed by several nitrogen freeze-pump-thaw cycles before admission into the spectrometers (PTB and UFSCar). Since the vapor pressure of THF reaches 170 Torr at room temperature, it was not necessary to heat the sample to vaporize the liquid. In the PTB setup, the injection line was preheated and kept at 50 °C before and during the injection to avoid THF condensation along the gas line, but this protocol was not necessary in the UFSCar setup due to the sufficient high room temperature.

III. RESULTS AND DISCUSSION

A. Absolute total ionization cross section

The absolute TICSs shown in Fig. 1 were measured ranging from 10 eV up to 1000 eV to benchmark previous experimental studies and theoretical models. The cross sections steeply rise from the 9.55 eV threshold[28] and peak at 14.5×10^{-16} cm^2 at around 80 eV electron energy, where it levels off and then steadily decays with increasing energy down to 3.9×10^{-16} cm^2 at 1000 eV. The present values are higher by a factor of 1.23, 1.15, 1.15, and 1.04 than the measurements by Bull *et al.*,[44] Fuss *et al.*,[20] Dampc *et al.*,[28] and Bug *et al.*,[25] respectively, but have very similar values compared to the data of Baek *et al.*[19] Dampc *et al.*[28] set the relative TICS to unity and compared with calculations of Mozejko and Sanche, Fuss *et al.*[20] put their relative values on an absolute scale by normalizing to the TICS of N_2, Bull *et al.*[25] determined the absolute TICS from a Beer-Lambert type law and Bug *et al.*[25] obtained absolute TICS by integration of measured double differential ionization cross sections. Baek *et al.*[19] measured absolute total inelastic cross sections, and the pure ionization cross sections were obtained by subtracting the contribution of the summed total excitation cross section reported

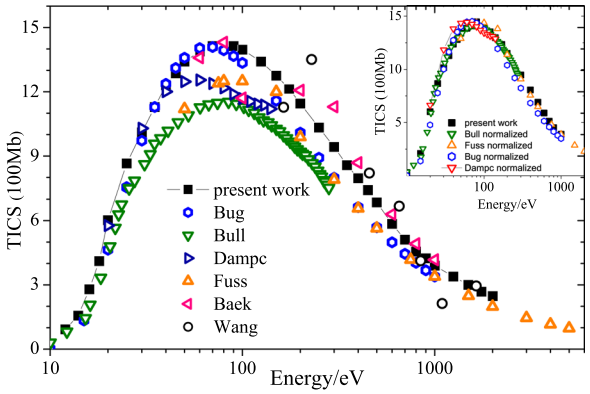

FIG. 1. THF total ionization cross section in 100 Mb (10^{-16} cm^2). Closed squares show the present work, open diamond data from Bug *et al.*,[25] open down-triangle data from Bull *et al.*,[44] open right-triangle data from Dampc *et al.*,[28] open up-triangle data from Fuss *et al.*,[20] open left-triangle data from Baek *et al.*,[19] and open circle data from proton impact at equivalent energy.[45] The inset shows TICS of Bull *et al.*, Fuss *et al.*, Dampc *et al.*, and Bug *et al.* multiplied by 1.23, 1.15, 1.15, and 1.04, respectively, for normalization on the maximum.

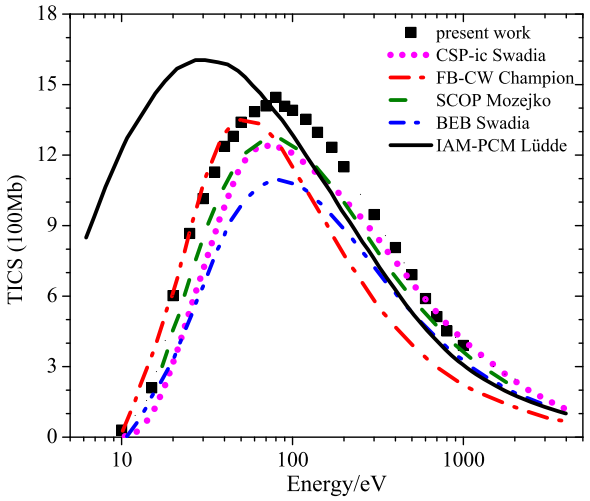

FIG. 2. Total ionization cross section in 100 Mb (10^{-16} cm^2) for electron impact on THF molecules. The closed squares show present experimental work, and calculations are depicted as the dotted line for CSP-ic by Swadia *et al.*,[23,24] the dashed-dotted line for FB-CW by Champion,[27] the dashed line for SCOP by Możejko *et al.*,[4] the dashed-dotted-dotted line for BEB by Swadia *et al.*,[23,24] and for proton impact on THF as the solid line for IAM-PCM by Lüdde *et al.*[26] Proton energies were scaled to equivalent electron energies, see text.

by Fuss *et al.*[20] The inelastic cross section tends to merge with the ionization data at higher energies beyond 1000 eV.[15,23] The inset in Fig. 1 shows the data normalized to the maximum of the present results indicating that the profiles of the TICS almost coincide.

The observed discrepancies of up to 20% in the absolute values might be due to the different experimental procedures applied to put the measured values on an absolute scale and unstable conditions. For instance, the detection efficiency in mass spectrometers and electron multiplier detectors, in particular, the loss of ions with high kinetic energy release (KER) and ions with low KER but high mass, has to be accounted for. In addition, a stable and reproducible number density is required, especially in nonvolatile and adsorbing samples[44] such as THF. When ion intensities are converted to absolute scale by normalizing to electron-impact ionization cross sections of reference gases,[20,44] equivalent conditions for the beam profiles in crossed beams are essential.[19,42]

In Fig. 2, the present TICSs are shown along with the theoretical results based on the spherical-complex-optical-potential (SCOP) model,[4] the Binary-Encounter-Bethe (BEB) framework,[23] the FBA-CW approximation,[27] and the complex-scattering-potential ionization-contribution formalism (CSP-ic).[23] In the energy range covered, the calculations exhibit a small variation at the peak energy but underestimate the present TICS throughout the energy range, except for the recent CSP-ic calculation from 300 to 1000 eV.[23]

In order to explore the role of the mass of the ionizing particle, the total cross section based on the IAM-PCM model[26] for proton collision is compared with the present experimental data for electron impact. For comparison, the proton energies were scaled to equivalent electron energies by multiplying with m_p/m_e, the ratio of the masses of proton and electron. The maxima of the proton and electron cross sections occur at different impact energies as shown for pyrimidine by Wolff *et al.*[29] At intermediate equivalent energies, the proton collision cross sections are lower relative to the present experimental electron impact cross section. It should be mentioned that at this intermediate range, the differences in the cross sections for equivelocity protons and electrons might be real and due to a charge-sign effect as reported for methane.[32] However, this issue can only be elucidated when proton measurements become available. A comparison within the theoretical models shows that at intermediate energies, the cross sections for electron impact based on the SCOP method[4,23,24] are higher than the proton cross sections calculated by the IAM-PCM model[26] and only at impact energies above 1 keV both experimental data and theoretical results appear to coincide.

B. Dissociative ionization cross sections

The high resolution time-of-flight spectrometer allows for the identification of a large number of cationic species, in total 43 fragment ions, the molecular parent-ion and two heavier ionic isotopes, and four dicationic fragments, revealing the complex fragmentation dynamics of THF. For example, Fig. 3 shows the mass spectrum recorded at 70 eV electron impact energy. The fragmentation pathways of THF were already discussed in the early works of Gallegos and Kiser[46] and Collin and Conde-Caprace.[47] They reported relative abundances of 17 fragment-ions at 70 eV and 14 ionic species from the threshold to 50 eV, respectively.

Figures 4(a)–4(f) present an overview of ionic species showing that upon ionization, THF produces a variety of ion species including successive losses of hydrogen atoms during molecular fragmentation. Most of the molecular parent ions produced are energetically unstable which dissociate into fragments by one or N-body breakups, through single or double ionization. The simplest

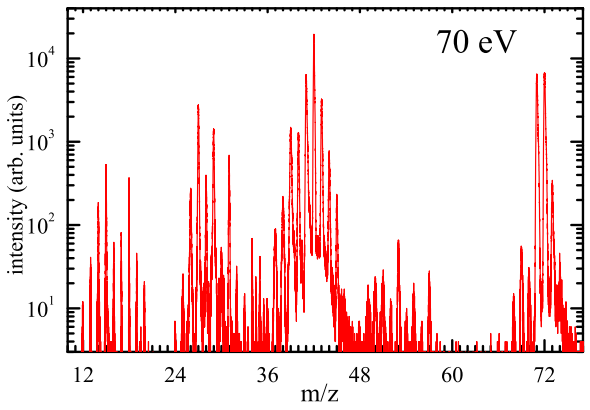

FIG. 3. THF mass spectrum at 70 eV electron impact energy obtained at PTB.

molecular cleavage is the breaking of the parent molecular ion into two parts—one of which carrying the positive charge and the other being an uncharged free radical.

The ratios of the partial dissociative ionization cross sections (PDCSs) of several fragment-ions are drawn relative to the ionization cross sections of the molecular parent ion, $C_4H_8O^+$ (PICS). Figures 4(a)–4(f) show the progressive dependence of the ratios on the electron energy, from an almost constant energy dependence for a wide range of electron energies [Fig. 4(a)] to a steep decrease starting around 150 eV electrons [Fig. 4(f)]. Figures 4(a)–4(f) also exhibit the correlation of the ratio's profile as a function of the impact energy with the ionic species production. Figure 4(a) displays the molecular parent ion losing up to six hydrogen atoms, $C_4H_{2-8}O^+$. On the other hand, larger fragment-ions, such as $C_{2-4}H_7^+$, can form bonding up to seven hydrogen atoms [see Figs. 4(b) and 4(c)]. The presence of ions with N-bonded carbon atoms, $C_{n=1-4}$ with three, then only

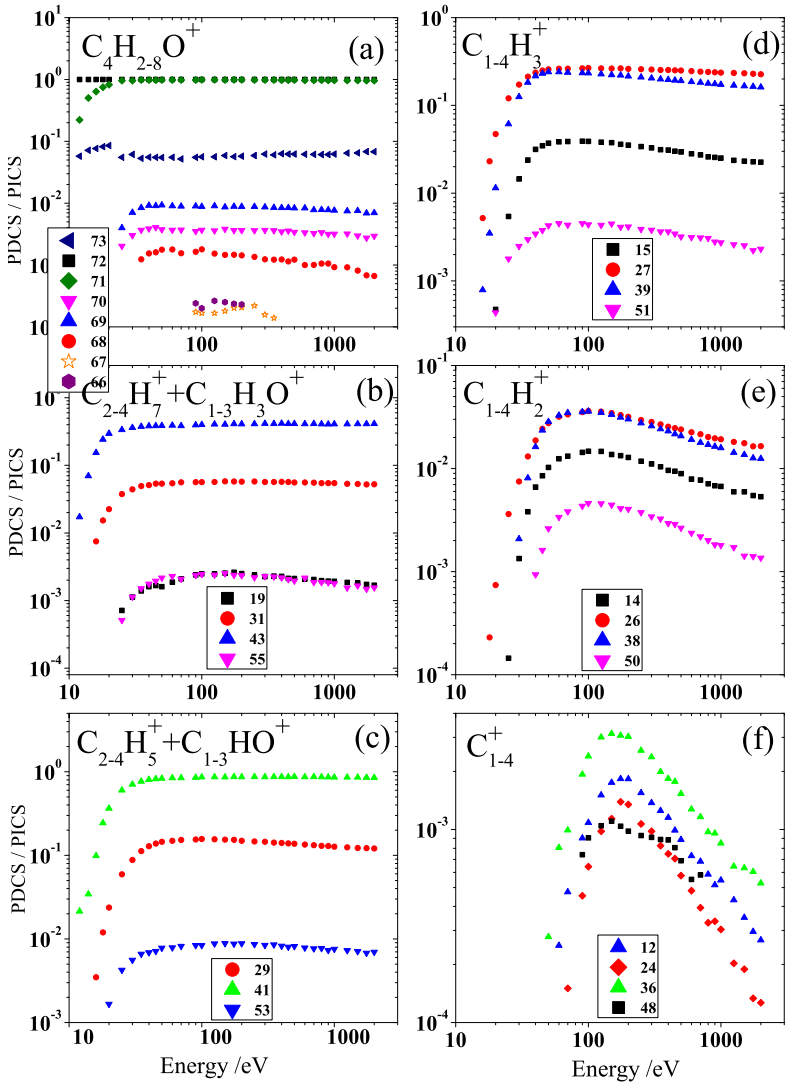

FIG. 4. Ratio between the partial dissociative ionization cross section (PDCS) of fragment-ions and the parent ion ionization cross section (PICS) of THF grouped for fragments with multiples of carbon and oxygen atoms with a fixed number of hydrogen atoms: (a) parent ion losing up to six hydrogen atoms $C_4H_{2-8}O^+$ and ionic fragments, (b) $C_{2-4}H_7^+$ + $C_{1-3}H_3O^+$, (c) $C_{2-4}H_5^+$ + $C_{1-3}HO^+$, (d) $C_{1-4}H_3^+$, (e) $C_{1-4}H_2^+$, and (f) bare C_{1-4}^+.

two hydrogen atoms [Figs. 4(d) and 4(e)] until bare of all hydrogen atoms, can be observed in Fig. 4(f).

The emission of up to two neutral hydrogen atoms by the parent ion is due to single ionization, but likely due to double ionization with N-breakups for larger numbers of emitted hydrogen atoms.[48] The formation of larger fragment-ions, as shown in Figs. 4(b) and 4(c), is due to the dominant single ionization with little contribution of direct double ionization. The fragment-ions composed of carbon atoms with a small number of hydrogen atoms [see Figs. 4(d)–4(f)] may originate from multibody breakup with the ejection of more than one ion (i.e., through double ionization) in coincidence with neutral fragments.[49] The steep decaying trend after the maximum of the ratios toward higher energies shown in Fig. 4(f) points out that the fragmentation predominantly proceeds through double ionization. These interpretations will be discussed in detail in the description of the semiempirical model. The absolute total ionization cross sections (TICSs), molecular parent-ion ionization cross sections (PICSs), and partial dissociation cross sections (PDCSs) of all measured cations as a function of the electron impact energy are listed in Tables S1–S4 of the supplementary material.

Experimental studies have previously reported PDCSs: Dampc *et al.*[28] presented PDCS for nine ionic species from 5 eV to 150 eV electron impact obtained by normalization of the partial yields to the theoretical calculation of Możejko *et al.*[4] at 70 eV. Fuss *et al.*[20] showed PDCS grouped due to limited mass/charge resolution in $C_nH_m^+$ and $C_{n-1}OH_m^+$ species over a wide range of electron impact energy from 50 eV to 5000 eV.

In order to estimate the impact of the valence shell ionization on the fragmentation pattern, we use the fragmentation matrix model that was successfully applied for smaller molecules, such as water,[30,33,50] methane,[32] and DNA base analogs.[29,34] In particular, we will discuss the single and double ionization of outer and inner valence shells, and K-shell ionization, involved in the fragment ion production as a function of the electron impact energy by means of the fragmentation matrix model (FMM).

C. Fragmentation production mechanisms

The relative contribution of the single ionization of each molecular orbital (MO) in the fragment-ion production was estimated by using an improved semiempiric fragmentation model that requires the following input parameters: absolute TICS and PDCS as a function of the energy, molecular orbital ionization energies (IPs), character of the molecular orbitals, appearance energies, and breakdown curves of the ionic species.

1. Molecular orbitals of THF and ionic species

According to calculations, three possible conformations, C_1, C_2, and C_s, are produced by pseudorotation of THF.[51–56] There is a competition between the THF conformers of C_2 and C_s structures in the gas phase and both of them coexist at room temperature. Fortunately, the orbital energies and MO characters of these two conformers resemble each other.[51–53,56–58] In the discussions that follow, the valence MOs are presented on the conformer of the C_2 type. Tetrahydrofuran possesses 30 valence electrons, which doubly occupy 15 orbitals in the electronic ground state: 9b, 11a, 10a, 8b, 9a, 7b, 6b, 8a, 7a, 5b, 6a, 4b, 3b, 5a, and 4a, where the first ten MOs form the outer valence shells with ionization potential below 18 eV, and the last five belong to the inner valence shells. Five more core shells complete the description of the THF molecule.[27] As an input parameter of the valence shell ionization energies (IPs), the average of the experimental energies was considered in the FMM and their values are included in Table I. The calculated IPs are systematically higher than the measured ones, including the first ionization potential.[51–53,58] The measured appearance energies of several ions, which correspond to the lowest energy for which the dissociation channels become accessible, are available in the literature.[28,46,59–61] However, the values extracted from ionic efficiency curves[28,46,59] are quite different than those obtained from breakdown curves and binding energy spectra.[60,61] In the process of constructing the fragmentation matrix, we chose as a reference the breakdown curves and the binding energy spectra measured by Mayer *et al.*[60] and Ren *et al.*,[61] respectively.

2. Principles and improvements of fragmentation matrix model

The fragmentation matrix model was described in detail by Montenegro *et al.*[30] and Wolff *et al.*,[29] and only a brief description is presented here. Accordingly, the single ionization cross section by electron impact for an arbitrary target shell or molecular orbital follows the simple scaling as a function of the electron impact energy E,[30]

$$\frac{\sigma_{nl}\, I_{nl}^2}{Z_{nl}\, \delta_{nl}} = F\left(\frac{E}{I_{nl}}\right), \tag{5}$$

with

$$F(x) = \frac{A\, ln(1 + B\, x)}{x} - \frac{A\, B}{(1 + C\, x)^2}, \tag{6}$$

where

$$x = \frac{1.836\, E(\text{eV})}{I_{nl}} - 24.97, \tag{7}$$

with A, B, and C as adjustable parameters, I_{nl} is the ionization potentials in units of rydbergs (13.6 eV), and σ_{nl} is the cross section. The label nl represents a particular molecular orbital. For all orbitals $Z_{nl} = 2$, $\delta_{nl} = 0.66$, and all parameters in Eqs. (5) and (6) are the same, except I_{nl}. The parameter δ_{nl} synthesizes the particular details of each atomic or molecular orbital and was adjusted to give the better general agreement with the measured total ionization cross section. A vacancy produced in a particular MO_{nl} has a probability $f_{m,nl}$ to give rise to a fragment-ion with mass m, and the set of fragmentation fractions defines the matrix based on the calculated cross section for single ionization of the MOs. The calculated TICS, σ_{nl}, is obtained by summation of the MOs' cross sections. The ionization potentials, the appearance energies and intensities, and limits of the breakdown curves restrain the options to fill the matrix, but still some freedom remains. The assignment is not unique and some freedom to change the tabulated values exists. If σ_{nl} is the cross section for a vacancy production in the MO_{nl}, the cross section σ_m to produce a fragment with mass m is given by the product of the fragmentation fractions (a matrix element) and the ionization cross sections of each molecular orbital where the valence hole is produced, that is,

TABLE I. Fragmentation matrix of 16 ionic species based on outer and inner valence shell MOs of THF [row 1: MO assignment on C_2 symmetry; row 2: ionization potential in eV of MOs; row 3: character of MOs; row 4: individual cross section of MOs calculated by FMM in Mb; column 1: mass species: 14 (CH_2^+), 15 (CH_3^+), 26 ($C_2H_2^+$), 27 ($C_2H_3^+$), 28 ($C_2H_4^+$), 29 (CHO^+), 31 (CH_3O^+), 37 (C_3H^+), 39 ($C_3H_3^+$), 40 ($C_3H_4^+$), 41 ($C_3H_5^+$), 42 ($C_3H_5^+$), 43 ($C_2H_3O^+$), 44 ($C_2H_3O^+$), 71 ($C_4H_7O^+$), and 72 ($C_4H_8O^+$); column 2: experimental cross section of ions for 400 eV electron impact in Mb; column 3: FMM summed cross section of individual MOs for 400 eV electron impact in Mb; and columns 4–18: contribution of each MOs to ion production], cross section expressed in Mb ≡ 10^{-18} cm^2.

		MO	9b	11a	10a	8b	9a	7b	8a	6b	7a	5b	6a	4b	3b	5a	4a
		IP-eV	9.7	11.73	12.0	12.48	12.71	14.18	14.48	15.35	16.63	16.70	18.77	19.48	23.40	24.60	31.80
		Char	nOper	nOpar+ CC	CH	CH+ CC	nOpar+ CH	CO+ CH	CH+ nO	CH+ COper	CH+ COpar	CH+ COper	CH + s-C	CH + s-C	s-C	s-C	s-O+ s-C
		CS-Mb	105.5	81.29	69.1	65.46	72.71	55.13	60.52	49.49	44.35	44.08	37.50	35.61	28.97	27.21	19.68
Mass	400 eV expt.	400 eV FMM															
72	135.0	117.7	0.9	0.28													
71	131.9	110.5	0.1	0.72	0.6												
44	13.7	11.5					0.03	0.05	0.06	0.06							
43	56.4	48.5				0.06	0.10	0.15	0.25	0.28							
42	232.3	212.0			0.4	0.94	0.87	0.74	0.31								
41	117.6	102.5						0.06	0.35	0.54	0.58	0.58					
40	23.0	20.0							0.01	0.04	0.14	0.12	0.09	0.07			
39	26.6	23.5									0.04	0.04	0.12	0.12	0.20	0.20	
37	1.6	0.8														0.01	0.03
31	7.7	6.3							0.02	0.04	0.03	0.04					
29	19.1	16.1								0.04	0.06	0.05	0.09	0.07	0.06	0.06	
28	5.3	4.3									0.02	0.03	0.03	0.02	0.01	0.01	
27	34.2	29.2									0.13	0.14	0.19	0.19	0.06	0.06	
26	3.4	2.3												0.01	0.02	0.03	0.03
15	4.2	3.1											0.01	0.02	0.03	0.03	0.03
14	1.3	0.8														0.01	0.02
Sum	813	710	1	1	1	1	1	1	1	1	1	1	0.53	0.50	0.38	0.40	0.11

$$\sigma_m = \sum_{nl} f_{m,nl}\sigma_{nl} \tag{8}$$

subject to the constraint

$$\sum_{nl} f_{m,nl} = 1. \tag{9}$$

The fragmentation matrix was constructed considering all 15 valence shell MOs of tetrahydrofuran in the C_2 conformation. Table I includes the ionization potential (eV), the character and the total ionization cross section of each MO in rows two, three, and four, respectively. These individual MOs' cross sections are distributed according to the matrix among the 16 selected fragment-ions with the highest experimental cross sections. Columns one, two, and three of Table I contain, for example, the m/z of the chosen fragment-ions with their measured and calculated cross sections by the FMM at an electron impact energy of 400 eV.

The PDCSs of 16 ionic fragment species were considered for the FMM analysis, namely, the fragment ions with cross sections with maxima higher than 350 Mb. A careful inspection revealed that the shape of the cross sections of some ionic species was quite distinguishable. Some of the cross sections show a faster rise with the impact energy, a higher appearance threshold (see fragment 27) or a cross section maximum shifted to lower impact energies (see fragment 42), so that an improvement of the model was required. It is not surprising that many of the ionic species correlate with the structure of the MOs and the bonding from which they originated. The characters of the MOs need to be included in the fragmentation matrix model.

In previous studies using the FMM,[29,34,50] a single set of free adjustable parameters (A, B, and C) was used to calculate the individual MO cross sections. Here, three sets of parameters were defined to take into account the major character of the MOs (see Table I row three). Two sets were defined for the outer valence shell MOs: one with $A = 16\,000$, $B = 0.012$, and $C = 0.004\,29$ related to the electronic density distribution on the oxygen atom in the ring (9b, 11a, 9a, 7b, and 8a), and a second with $A = 12\,500$, $B = 0.016$, and $C = 0.007\,62$ for the C–H and C–C bonds (10a, 8b, 6b, 7a, 5b, 6a, and 4b). The third set ($A = 7500$, $B = 0.08$, and $C = 0.013\,33$) was dedicated to the dominant inner valence shell MOs (3b, 5a, and 4a). With these values of A, B, and C, Eq. (5) gives σ_{nl} in units of Mb (10^{-18} cm^2). The computed molecular orbitals allowed for comparison and defining these sets by the preferential location of the electrons in the MO.[51,56,60] The electron distribution of the 9b orbital is mostly on the oxygen atom, 11a extends along the C–O–C plane but still around the oxygen atom, 9a has larger exterior distribution on the oxygen atom, and 6b extends outside around the hydrogen atoms and the oxygen atom. The electrons of the higher valence MOs (10a, 8b, 7b, 6b, 7a, 5b, 6a, and 4b) are essentially located around hydrogen of beta or alpha-carbon atoms (C–H bonds) or extends outside the C–O–C plane. The s-orbital character of the C and O atoms in the ring dominates the last three inner valence orbitals (3b, 5a, and 4a).

3. Absolute dissociative ionization cross sections and fragmentation matrix model predictions

Figures 5(a) and 5(b) show a comparison between experimental data and calculated FMM results. For most of the selected fragment ions, the cross sections obtained with the FMM agree well with the experimental values over the entire energy range. The fragmentation matrix model was evaluated by taking the ratio between the FMM cross sections and the experimental cross sections, as shown in the insets in Figs. 5(a) and 5(b). The deviation from unity of the ratio gives a quantitative measure of the ionization mechanisms involved in the fragment-ion production. Within a small deviation (±0.1) from unity, the model based only on the fragmentation following single ionization is suitable describing the fragment-ion production. The ionic species here considered belong to the ions grouped in Figs. 4(a)–4(c) produced mostly with high abundances. The good agreement between the experimental and FMM cross section shown in Fig. 5(a) demonstrates that this improved FMM is a reliable tool to estimate the contribution of the valence shell single ionization in the fragment-ion production of complex molecules.

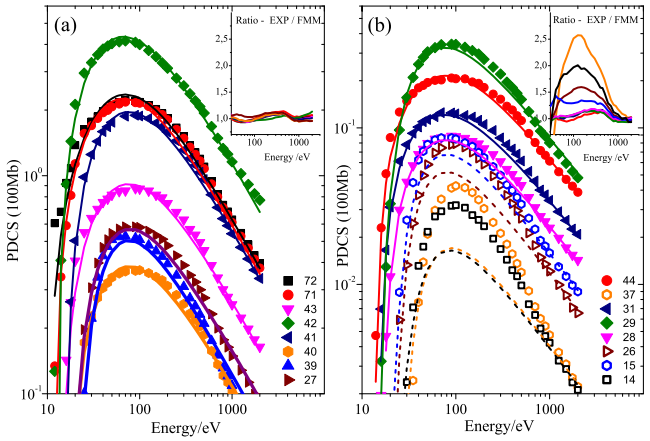

FIG. 5. Experimental partial dissociation cross section (PDCS) denoted by symbols and the corresponding fragmentation matrix model calculations indicated by lines for fragments with (a) high and (b) low cross sections. Fragments with calculated PDCS below 70 Mb are drawn in dashed lines. Insets in (a) and (b) show the ratio between the experimental and calculated PDCS.

4. Single and double ionization contribution

There are, however, clear deviations from the model prediction that correlate with processes not considered in the model. Figure 5(b) illustrates that FMM prediction does not properly describe the production of the fragment-ions CH_2^+, CH_3^+, $C_2H_2^+$, and C_3H^+ ($m/z = 14$, 15, 26, and 37) except for high electron impact energies, where the single ionization dominates. These deviations suggest more complex or high-order vacancy-production mechanisms, such as double ionization, which contribute to the fragmentation. These second order processes enhance the cross section near its maximum and in the intermediate electron energy range. The energy-dependent ratios of the ionic species already shown in Figs. 4(d)–4(f) follow clearly these observed features. The breakdown curves of ionized THF[60] indicate that these ions can be formed from single ionization of the inner valence shells, particularly the cations C_3H^+ and $C_3H_2^+$ ($m/z = 37$ and 38) by removing an electron of the carbon or oxygen 2s shells. But in this energy range, THF can also

be directly doubly ionized (double ionization threshold is at 23.2 eV and 26.2 eV[60]) and form two ionic species, like the cations CH_3^+, CH_4^+ or O^+, OH^+, CH_3^+, $C_2H_2^+$, C_3H^+ and $C_3H_2^+$ (m/z = 15–17, 26, 37, and 38), and possibly additional neutral fragments.

Figures 6(a) and 6(b) display the ratios of the fragment cross sections to the parent ion cross section of the ionic species considered in Figs. 5(a) and 5(b), with symbols indicating the experimental ratios and solid lines the ratios calculated by the FMM. From Figs. 6(a) and 6(b), two main trends are identified: in Fig. 6(a), after the cross section maximum, the experimental ratios for all displayed m/z fragments are almost constant up to the highest electron energy at 2000 eV suggesting that the single ionization is dominant, and the double ionization processes can be neglected. In Fig. 6(b), the experimental ratios reach a maximum and decrease, while the ratios predicted by the FMM remain constant. The calculated ratios indicated as solid lines, included in Figs. 6(a) and 6(b), highlight the differences in the fragmentation process. A slow decrease of the measured ratio toward high energies implies that double ionization processes are present, but not dominant, as shown for the fragments $C_2H_3^+$, CHO^+, and $C_3H_3^+$ (m/z = 27, 29, and 39). Otherwise, a steep decrease of the measured ratio indicates that the double ionization is prominent and mostly responsible for the fragment-ion production in the intermediate electron impact range as illustrated for the ionic species CH_2^+ and C_3H^+ (m/z = 14 and 37). The argument that the double ionization and multiple-body fragmentation are taking place corroborates with the much broader kinetic energy distributions (KEDs) of the fragment-ions $C_2H_3^+$, CHO^+, and $C_3H_3^+$ (m/z = 27, 29, and 39) than those of the ions $C_3H_5^+$, $C_3H_6^+$, $C_2H_3O^+$, and $C_4H_7^+O$ (m/z = 41–43 and 71).[61] The magnitudes and shapes of the KEDs are quite different for the two sets of ions, for example, the averaged kinetic energy measured by Ren *et al.* for the most abundant ion in the fragmentation of THF, namely, $C_3H_6^+$ (m/z = 42) is 39 meV, while for the ion $C_3H_3^+$ (m/z = 39) is 150 meV.[61]

To be more specific about the energy-dependent cross sections or ratios of some particular fragment-ions with similar masses, based on the observed features shown in Figs. 6(a) and 6(b), we can say that ethylene ions $C_2H_4^+$ (m/z = 28) are produced mostly by single ionization, while acetylene ions $C_2H_2^+$ (m/z = 26) by double ionization. Although both ions have approximately similar cross section values around the maximum at 80 eV electron impact energy, the acetylene ions' cross section is two times smaller than that of ethylene ions at around 1000 eV electron impact energy. This illustrates that for some ionic species care should be taken when extrapolating dissociation cross sections to higher impact energies due to energy-dependence on the ionization mechanisms involved in its production.

5. Post collisional processes

The role of the K-shell Auger process in the double ionization can be estimated through the ratios of K-shell ionization and single ionization of THF cross sections, included in Fig. 6(a). The K-shell cross sections were obtained by summing up the carbon and oxygen K-shell cross sections.[62] The ratio reaches almost 2.5% at 2000 eV suggesting that the K-shell contribution might not be negligible in the production of some ionic species. Auger processes would be indicated by a flattening in the ratio profile of some fragments toward a constant value, which is, however, absent within the covered energy range, while it was clearly evident in the case of the electron impact ionization on water and methane.[30–32] Full molecular fragmentation induced by single ionization of water and methane[32,63] is also dominated by satellite states with energies close to those corresponding to a vacancy in an inner valence orbital. These satellite states induce multiple hydrogen ejections.[32,64,65] Shake-up satellites in the C 1s electron spectra have been reported in some organic moieties by Pignataro *et al.*,[66] but satellite structures were absent in the analogous spectra of the corresponding alkyl and saturated derivatives, including tetrahydrofuran.[66] The data show significant differences between saturated and aromatic compounds.[66–68]

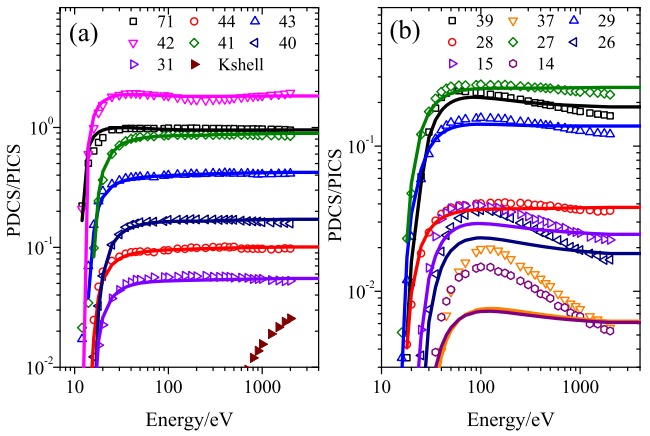

FIG. 6. Partial dissociation cross section (PDCS) divided by parent ionization cross section (PICS). The open symbols show experimental ratios and solid lines the FMM ratios for (a) fragments-ions CH_3O^+, $C_3H_4^+$, $C_3H_5^+$, $C_3H_6^+$, $C_2H_3O^+$, $C_2H_4O^+$, and $C_4H_7O^+$ (m/z = 31, 40–44, and 71), including calculated K-shell ratio and (b) fragment-ions CH_2^+, CH_3^+, $C_2H_2^+$, $C_2H_3^+$, $C_2H_4^+$ or CO^+, CHO^+, C_3H^+ and $C_3H_3^+$ (m/z = 14, 15, 26–29, 37, and 39).

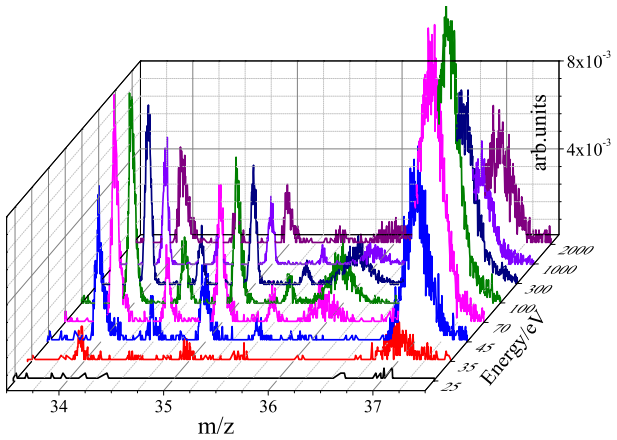

FIG. 7. Mass spectra in the m/z range of 34–37 showing the dicationic ions $C_4H_4O^{2+}$, $C_4H_5O^{2+}$, $C_4H_6O^{2+}$, and $C_4H_7O^{2+}$ (m/z = 34, 34.5, 35, and 35.5), and the cations C_3^+ and C_3H^+ (m/z = 36 and 37) for several electron impact energies: 25, 35, 45, 70, 100, 300, 1000, and 2000 eV. The mass spectral intensities were normalized on the peak intensity of the molecular parent ion $C_4H_8O^+$.

TABLE II. Fragmentation matrix extracted from Ren *et al.*[61] (left) and present work (right) shows the contribution of each MO to the fragment ion production. Row one shows the *m*/*z* of the ion species 72 ($C_4H_8O^+$), 71 ($C_4H_7O^+$), 42 ($C_3H_6^+$), 41 ($C_3H_5^+$), 39 ($C_3H_3^+$), 43 ($C_2H_3O^+$), 27 ($C_2H_3^+$), 29 (CHO^+), and 31 (CH_3O^+), and column one the outer and inner valence MOs of THF.

Ren *et al.* fragmentation matrix										Present work fragmentation matrix									
MO	72	71	42	41	39	43	27	29	31	MO	72	71	42	41	39	43	27	29	31
9b	0.80	0.20								9b	0.90	0.10							
11a		0.68	0.32							11a	0.28	0.72							
10a			0.88			0.12				10a		0.60	0.40						
8b			0.84			0.12			0.03	8b			0.94			0.06			
9a			0.84			0.13			0.03	9a			0.87			0.10			
7b				0.84		0.15			0.01	7b			0.74	0.06		0.15			
8a				0.43		0.27	0.28		0.02	8a			0.31	0.35		0.25			0.02
6b				0.72			0.13	0.13	0.02	6b				0.54		0.28		0.04	0.04
7a					0.23		0.52	0.19	0.06	7a				0.58	0.04		0.13	0.06	0.03
5b					0.23		0.52	0.19	0.06	5b				0.58	0.04		0.14	0.05	0.04
6a					0.63		0.37			6a					0.12		0.19	0.09	
4b					0.63		0.37			4b					0.12		0.19	0.07	
3b										3b					0.20		0.06	0.06	
5a										5a					0.20		0.06	0.06	

D. Tetrahydrofuran dications

Ion spectra recorded at electron impact energies ranging from 25 eV to 2000 eV electron are shown in Fig. 7. As the reflectron spectrometer was operated for high mass resolution with narrow peak widths, it was possible to identify dications by the width of the ion peaks: the peak widths associated with the dicationic ions $C_4H_4O^{2+}$, $C_4H_5O^{2+}$, $C_4H_6O^{2+}$, and $C_4H_7O^{2+}$ (m/z = 34, 34.5, 35, and 35.5) are narrower than the neighboring peaks of the fragment-ions C_3^+ and C_3H^+ (m/z = 36 and 37). The stable dicationic fragments $C_4H_{n=4-7}O^{2+}$ are formed by double ionization of the THF molecule (C_4H_8O) with loss of only hydrogen atoms attached to the ring. These dications gain little kinetic energy in their formation process compared to the kinetic energies of the fragment-ions that result from cleavage of the ring. The peak width reflects the kinetic energy release of the fragment ions and can be used to identify long-lived metastable dications. Mayer *et al.* calculated optimized structures for the THF dication ($C_4H_8O^{2+}$) and the expected appearance energies are 23.2 eV and 26.2 eV,[60] but in the present work, the doubly ionized parent ion is not at all discernible being buried under the fragment-ion C_3^+. Previous studies support the suggestion of Mayer *et al.* that the THF dication may be a short-lived transient metastable ion, decaying by fast fragmentation into two singly charged species plus one neutral species resulting in a negligible abundance. It should be mentioned that the unsaturated analog molecule, furan (C_4H_4O), produces doubly charged molecular parent ions with a large abundance.[48,69] Momentum spectroscopy with a reaction microscope[61,70] or the DETOF technique[71,72] could discriminate the ions species of the m/z = 36 peak and confirm the absence or measure the small abundance of $C_4H_8O^{2+}$.

E. Fragmentation matrix: Experiments and model

A fragment-ion can be formed from the single ionization of more than one molecular orbital, and the single ionization of a MO can produce different ionic species [see Eq. (8)]. The experimental results of Ren *et al.*[61] were found to be the most suitable to compare with the present FMM analysis, as the fragment ions were collected in coincidence with the ejected electron energies. The valence shells leading to specific ions were identified from the two-dimensional plot of the binding energy spectra vs m/z of the fragment ions. Unfortunately, the electron impact experiments were done at an energy of 26 eV only.[61] Besides this limitation, within the uncertainty, the present evaluation for the parent and nine fragment ions is coherent with Ren *et al.* data, as listed in Table II. For example, using FMM, the formation of the dehydrogenated parent ion was attributed to the ionization of the first two outer valence shells, 9b and 11a, as suggested by Ren *et al.*, in contradiction to previous appearance energy measurements.[28,60] As the electron impact energy increases, more fragmentation channels open up, the competition between the fragment channels enhances, and the contribution of the inner valence shell MOs increases.

IV. CONCLUSIONS

Experimental data of tetrahydrofuran obtained at two separate setups (high resolution TOF-MS and RFT) were used to assess the ionization induced by charged particles in the fragment-ion formation at the molecular level. The absolute total ionization cross section exceeds most of the theoretical cross section calculations below 300 eV but shows good agreement at higher energies. The absolute

partial dissociative ionization cross section of several fragment-ions, comprising up to 43 species, and the absolute ionization cross section of the molecular parent-ion and of two heavier ionic isotopes were presented showing a broad range of abundances. The wide electron impact range allowed for detailed analysis including various energy-dependent processes.

We discussed the ionization and fragmentation following ionization data with focus on the fragment-ion production mechanisms. The consistency of the fragmentation matrix model based on the single ionization was tested for 16 fragment-ions and against experimental results obtained by the reaction microscope technique. It was possible to discriminate the ionic species formed mainly by single ionization or due to both single and double ionization. The improved fragmentation matrix model taking into account the character of the MOs provides better performance on the description of the dissociation cross sections than the previous FMM over the measured range of electron impact energies. It has successfully predicted the contribution of the individual valence shell MOs on the fragment-ion production of the ionic species with high abundances. On the other hand, clear deviations between experimental and calculated cross sections found in the intermediate electron impact energy region pointed out the presence of the double ionization. The contribution of the double ionization processes and of the N-body breakup was recognized through the ratio of measured and calculated PDCSs relative to the molecular parent ion cross section. The relative dissociative ionization cross sections are sensitive on the ionization mechanisms dependent on the projectile energy, as was found for ethylene compared to acetylene. Therefore, extrapolation of the cross sections to higher electron impact energies than measured should be taken with care. Contribution of postcollisional processes, such as Auger and shake-up mechanisms in the fragment-ion production, was considered negligible in the measured electron impact range.

Additionally, the high resolution mass spectroscopy allowed for the identification of four doubly charged ions, but the dication of tetrahydrofuran was not observed and it is likely to undergo fast fragmentation in contrast to the more stable dication of unsaturated furan. Future works at higher energies and under impact of positive charged ions are called for to clarify the contribution of second order processes and of effect of the charge-sign of projectile in THF fragment-ion production.

SUPPLEMENTARY MATERIAL

See supplementary material for the cross section data of all measured cations, listed in Tables S1–S4, TICS data listed in Table S5, and the ionic species assignment of m/z in Table S6.

ACKNOWLEDGMENTS

This research was supported by the Brazilian agencies CNPq, CAPES (Finance Code 001), FAPESP (Grant No. 2015/08258-2), and by the PTB. W.W. wishes to thank the staff of PTB's Ionizing Radiation Division for their valuable support. M.G.P.H. wishes to thank Professor Ione Iga for construction of the spectrometer used at UFSCar.

REFERENCES

[1] H. Nikjoo, P. O'Neill, M. Terrissol, and D. T. Goodhead, "Quantitative modelling of DNA damage using Monte Carlo track structure method," Radiat. Environ. Biophys. **38**(1), 31–38 (1999).
[2] B. Boudaïffa, D. Hunting, P. Cloutier, M. A. Huels, and L. Sanche, "Induction of single- and double-strand breaks in plasmid DNA by 100–1500 eV electrons," Int. J. Radiat. Biol. **76**(9), 1209–1221 (2000).
[3] W. M. Huo, C. E. Dateo, and G. D. Fletcher, "Molecular data for a biochemical model of DNA damage: Electron impact ionization and dissociative ionization cross sections of DNA bases and sugar-phosphate backbone," Radiat. Meas. **41**(9), 1202–1208 (2006).
[4] P. Możejko, E. Ptasińska-Denga, A. Domaracka, and C. Szmytkowski, "Absolute total cross-section measurements for electron collisions with tetrahydrofuran," Phys. Rev. A **74**, 012708 (2006).
[5] A. K. Ghosh and D. D. Anderson, "Tetrahydrofuran, tetrahydropyran, triazoles and related heterocyclic derivatives as HIV protease inhibitors," Future Med. Chem. **3**(9), 1181–1197 (2011).
[6] M. G. P. Homem, R. T. Sugohara, I. P. Sanches, M. T. Lee, and I. Iga, "Cross sections for elastic electron collisions with tetrahydrofuran," Phys. Rev. A **80**, 032705 (2009).
[7] A. Zecca, C. Perazzolli, and M. J. Brunger, "Positron and electron scattering from tetrahydrofuran," J. Phys. B: At., Mol. Opt. Phys. **38**(13), 2079–2086 (2005).
[8] D. Bouchiha, J. D. Gorfinkiel, L. G. Caron, and L. Sanche, "Low-energy electron collisions with tetrahydrofuran," J. Phys. B: At., Mol. Opt. Phys. **39**(4), 975–986 (2006).
[9] C. Winstead and V. McKoy, "Low-energy electron scattering by deoxyribose and related molecules," J. Chem. Phys. **125**(7), 074302 (2006).
[10] C. J. Colyer, V. Vizcaino, J. P. Sullivan, M. J. Brunger, and S. J. Buckman, "Absolute elastic cross-sections for low-energy electron scattering from tetrahydrofuran," New J. Phys. **9**(2), 41 (2007).
[11] M. Allan, "Absolute angle-differential elastic and vibrational excitation cross sections for electron collisions with tetrahydrofuran," J. Phys. B: At., Mol. Opt. Phys. **40**(17), 3531–3544 (2007).
[12] M. Dampc, I. Linert, A. R. Milosavljević, and M. Zubek, "Vibrational excitation of tetrahydrofuran by electron impact in the low energy range," Chem. Phys. Lett. **443**(1), 17–21 (2007).
[13] A. Gauf, L. R. Hargreaves, A. Jo, J. Tanner, M. A. Khakoo, T. Walls, C. Winstead, and V. McKoy, "Low-energy electron scattering by tetrahydrofuran," Phys. Rev. A **85**, 052717 (2012).
[14] L. Chiari, E. Anderson, W. Tattersall, J. R. Machacek, P. Palihawadana, C. Makochekanwa, J. P. Sullivan, G. García, F. Blanco, R. P. McEachran, M. J. Brunger, and S. J. Buckman, "Total, elastic, and inelastic cross sections for positron and electron collisions with tetrahydrofuran," J. Chem. Phys. **138**(7), 074301 (2013).
[15] M. C. Fuss, A. G. Sanz, F. Blanco, P. Limão-Vieira, M. J. Brunger, and G. García, "Differential and integral electron scattering cross sections from tetrahydrofuran (THF) over a wide energy range: 1–10 000 eV," Eur. Phys. J. D **68**(6), 161 (2014).
[16] M. J. E. Casey, J. de Urquijo, L. N. Serkovic Loli, D. G. Cocks, G. J. Boyle, D. B. Jones, M. J. Brunger, and R. D. White, "Self-consistency of electron-THF cross sections using electron swarm techniques," J. Chem. Phys. **147**(19), 195103 (2017).
[17] L. Zhang, W. Sun, Y. Zhang, Z. Fan, S. Hu, and Q. Fan, "Predicting differential cross sections of electron scattering from tetrahydrofuran," J. Phys. B: At., Mol. Opt. Phys. **50**(8), 085201 (2017).
[18] M. Dampc, A. R. Milosavljević, I. Linert, B. P. Marinković, and M. Zubek, "Differential cross sections for low-energy elastic electron scattering from tetrahydrofuran in the angular range 20°–180°," Phys. Rev. A **75**, 042710 (2007).
[19] W. Y. Baek, M. Bug, H. Rabus, E. Gargioni, and B. Grosswendt, "Differential elastic and total electron scattering cross sections of tetrahydrofuran," Phys. Rev. A **86**, 032702 (2012).
[20] M. Fuss, A. Muñoz, J. C. Oller, F. Blanco, D. Almeida, P. Limão Vieira, T. P. D. Do, M. J. Brunger, and G. García, "Electron-scattering cross sections for collisions with tetrahydrofuran from 50 to 5000 eV," Phys. Rev. A **80**, 052709 (2009).

[21]C. Limbachiya, M. Vinodkumar, M. Swadia, K. Joshipura, and N. Mason, "Electron-impact total cross sections for inelastic processes for furan, tetrahydrofuran and 2,5-dimethylfuran," Mol. Phys. **113**(1), 55–62 (2015).
[22]N. A. Garland, M. J. Brunger, G. Garcia, J. de Urquijo, and R. D. White, "Transport properties of electron swarms in tetrahydrofuran under the influence of an applied electric field," Phys. Rev. A **88**, 062712 (2013).
[23]M. Swadia, Y. Thakar, M. Vinodkumar, and C. Limbachiya, "Theoretical electron impact total cross sections for tetrahydrofuran (C_4H_8O)," Eur. Phys. J. D **71**(4), 85 (2017).
[24]M. Swadia, R. Bhavsar, Y. Thakar, M. Vinodkumar, and C. Limbachiya, "Electron-driven processes for furan, tetrahydrofuran and 2,5-dimethylfuran," Mol. Phys. **115**(20), 2521–2527 (2017).
[25]M. U. Bug, W. Y. Baek, H. Rabus, C. Villagrasa, S. Meylan, and A. B. Rosenfeld, "An electron-impact cross section data set (10 eV-1 keV) of DNA constituents based on consistent experimental data: A requisite for Monte Carlo simulations," Radiat. Phys. Chem. **130**, 459–479 (2017).
[26]H. J. Lüdde, A. Achenbach, T. Kalkbrenner, H.-C. Jankowiak, and T. Kirchner, "An independent-atom-model description of ion-molecule collisions including geometric screening corrections," Eur. Phys. J. D **70**(4), 82 (2016).
[27]C. Champion, "Quantum-mechanical predictions of electron-induced ionization cross sections of DNA components," J. Chem. Phys. **138**(18), 184306 (2013).
[28]M. Dampc, E. Szymańska, B. Mielewska, and M. Zubek, "Ionization and ionic fragmentation of tetrahydrofuran molecules by electron collisions," J. Phys. B: At., Mol. Opt. Phys. **44**(5), 055206 (2011).
[29]W. Wolff, H. Luna, L. Sigaud, A. C. Tavares, and E. C. Montenegro, "Absolute total and partial dissociative cross sections of pyrimidine at electron and proton intermediate impact velocities," J. Chem. Phys. **140**(6), 064309 (2014).
[30]E. C. Montenegro, "Fragmentation of water by heavy ions," J. Phys.: Conf. Ser. **194**(1), 012049 (2009).
[31]A. C. Tavares, H. Luna, W. Wolff, and E. C. Montenegro, "Double ionization of water molecules induced by swift protons," Phys. Rev. A **92**, 032714 (2015).
[32]H. Luna, W. Wolff, E. C. Montenegro, and L. Sigaud, "CH_4 fragmentation from single and double ionization by proton and electron impact," Phys. Rev. A **99**, 012709 (2019).
[33]E. Montenegro, L. Sigaud, W. Wolff, H. Luna, and N. Ferreira, "Some dynamical features of molecular fragmentation by electrons and swift ions," Phys. Procedia **66**, 39 (2015).
[34]W. Wolff, H. Luna, and E. C. Montenegro, "Isomeric signatures in the fragmentation of pyridazine and pyrimidine induced by fast ion impact," J. Chem. Phys. **143**(4), 044314 (2015).
[35]B. Rudek, A. Arndt, D. Bennett, M. Wang, and H. Rabus, "Ion induced fragmentation cross-sections of DNA constituents," Eur. Phys. J. D **69**(10), 237 (2015).
[36]F. Fantuzzi, B. Rudek, W. Wolff, and M. A. C. Nascimento, "Doubly and triply charged species formed from chlorobenzene reveal unusual C–Cl multiple bonding," J. Am. Chem. Soc. **140**(12), 4288–4292 (2018).
[37]F. d. A. Ribeiro, B. Rudek, H. B. A. Cerqueira, R. R. Oliveira, A. B. Rocha, M. L. M. Rocco, and W. Wolff, "Fragment and cluster ions from gaseous and condensed pyridine produced under electron impact," Phys. Chem. Chem. Phys. **20**, 25762–25771 (2018).
[38]S. K. Srivastava, A. Chutjian, and S. Trajmar, "Absolute elastic differential electron scattering cross sections in the intermediate energy region. I.–H_2," J. Chem. Phys. **63**(6), 2659–2665 (1975).
[39]H. C. Straub, P. Renault, B. G. Lindsay, K. A. Smith, and R. F. Stebbings, "Absolute partial and total cross sections for electron-impact ionization of argon from threshold to 1000 eV," Phys. Rev. A **52**, 1115–1124 (1995).
[40]R. Rejoub, B. G. Lindsay, and R. F. Stebbings, "Determination of the absolute partial and total cross sections for electron-impact ionization of the rare gases," Phys. Rev. A **65**, 042713 (2002).
[41]J. C. Nickel, P. W. Zetner, G. Shen, and S. Trajmar, "Principles and procedures for determining absolute differential electron-molecule (atom) scattering cross sections," J. Phys. E: Sci. Instrum. **22**(9), 730–738 (1989).
[42]M. G. P. Homem, I. Iga, R. T. Sugohara, I. P. Sanches, and M. T. Lee, "Role of adsorption effects on absolute electron-molecule cross-section calibration using the relative flow technique," Rev. Sci. Instrum. **82**(1), 013109 (2011).
[43]H. C. Straub, P. Renault, B. G. Lindsay, K. A. Smith, and R. F. Stebbings, "Absolute partial cross sections for electron-impact ionization of H_2, N_2, and O_2 from threshold to 1000 eV," Phys. Rev. A **54**, 2146–2153 (1996).
[44]J. N. Bull, J. W. L. Lee, and C. Vallance, "Absolute electron total ionization cross-sections: Molecular analogues of DNA and RNA nucleobase and sugar constituents," Phys. Chem. Chem. Phys. **16**, 10743–10752 (2014).
[45]M. Wang, B. Rudek, D. Bennett, P. de Vera, M. Bug, T. Buhr, W. Y. Baek, G. Hilgers, and H. Rabus, "Cross sections for ionization of tetrahydrofuran by protons at energies between 300 and 3000 keV," Phys. Rev. A **93**, 052711 (2016).
[46]E. J. Gallegos and R. W. Kiser, "Electron impact spectroscopy of the four- and five-membered, saturated heterocyclic compounds containing nitrogen, oxygen and sulfur," J. Phys. Chem. **66**(1), 136–145 (1962).
[47]J. Collin and G. Conde-Caprace, "Ionization and dissociation of cyclic ethers by electron impact," Int. J. Mass Spectrom. Ion Phys. **1**(3), 213–225 (1968).
[48]E. Erdmann, M. Łabuda, N. F. Aguirre, S. Díaz-Tendero, and M. Alcamí, "Furan fragmentation in the gas phase: New insights from statistical and molecular dynamics calculations," J. Phys. Chem. A **122**(16), 4153–4166 (2018).
[49]E. Erdmann, M.-C. Bacchus-Montabonel, and M. Łabuda, "Modelling charge transfer processes in C^{2+}-tetrahydrofuran collision for ion-induced radiation damage in DNA building blocks," Phys. Chem. Chem. Phys. **19**, 19722–19732 (2017).
[50]E. C. Montenegro, A. Tavares, H. Luna, and W. Wolff, "Inner valence-shell vacancy production and molecular fragmentation," J. Phys.: Conf. Ser. **635**, 012019 (2015).
[51]M. Yamauchi, H. Yamakado, and K. Ohno, "Penning ionization of cyclic ethers by collision with $He^*(2^3S)$ metastable atoms," J. Phys. Chem. A **101**(35), 6184–6194 (1997).
[52]C. G. Ning, Y. R. Huang, S. F. Zhang, J. K. Deng, K. Liu, Z. H. Luo, and F. Wang, "Experimental and theoretical electron momentum spectroscopic study of the valence electronic structure of tetrahydrofuran under pseudorotation," J. Phys. Chem. A **112**(44), 11078–11087 (2008).
[53]T. Yang, G. Su, C. Ning, J. Deng, F. Wang, S. Zhang, X. Ren, and Y. Huang, "New diagnostic of the most populated conformer of tetrahydrofuran in the gas phase," J. Phys. Chem. A **111**(23), 4927–4933 (2007).
[54]A. Giuliani, P. Limão-Vieira, D. Duflot, A. R. Milosavljevic, B. P. Marinkovic, S. V. Hoffmann, N. Mason, J. Delwiche, and M.-J. Hubin-Franskin, "Electronic states of neutral and ionized tetrahydrofuran studied by VUV spectroscopy and *ab initio* calculations," Eur. Phys. J. D **51**(1), 97–108 (2009).
[55]J. D. Builth-Williams, S. M. Bellm, L. Chiari, P. A. Thorn, D. B. Jones, H. Chaluvadi, D. H. Madison, C. G. Ning, B. Lohmann, G. B. da Silva, and M. J. Brunger, "A dynamical (e,2e) investigation of the structurally related cyclic ethers tetrahydrofuran, tetrahydropyran, and 1,4-dioxane," J. Chem. Phys. **139**(3), 034306 (2013).
[56]P. Duffy, J. A. Sordo, and F. Wang, "Valence orbital response to pseudorotation of tetrahydrofuran: A snapshot using dual space analysis," J. Chem. Phys. **128**(12), 125102 (2008).
[57]C. Colyer, S. Bellm, B. Lohmann, G. Hanne, O. Al-Hagan, D. Madison, and C. Ning, "Dynamical (e,2e) studies using tetrahydrofuran as a DNA analog," J. Chem. Phys. **133**(12), 124302 (2010).
[58]H. Bock, "K. Kimura, S. Katsumata, Y. Achiba, T. Yamazaki and S. Iwata: Handbook of He photoelectron spectra of fundamental organic molecules: Ionization energies, *ab initio* assignments, and valence electronic structure for 200 molecules. Japan Scientific Societies Press, Tokyo und Halstead Press, New York, 1981," Ber. Bunsengesellschaft Phys. Chem. **86**(3), 266 (1982).
[59]G. Conde-Caprace and J. E. Collin, "Ionization and dissociation of cyclic ethers and thioethers by electron-impact. A comparison between 1,3-dioxolane, 1,3-dithiolane and 1,3-oxathiolane," Org. Mass Spectrom. **6**(4), 415–423 (1972).
[60]P. M. Mayer, M. F. Guest, L. Cooper, L. G. Shpinkova, E. E. Rennie, D. M. P. Holland, and D. A. Shaw, "Does tetrahydrofuran ring open upon ionization and dissociation? A TPES and TPEPICO investigation," J. Phys. Chem. A **113**(41), 10923–10932 (2009).

[61]X. Ren, T. Pflüger, M. Weyland, W. Y. Baek, H. Rabus, J. Ullrich, and A. Dorn, "An (e, 2e + ion) study of low-energy electron-impact ionization and fragmentation of tetrahydrofuran with high mass and energy resolutions," J. Chem. Phys. **141**(13), 134314 (2014).
[62]X. Llovet, C. J. Powell, F. Salvat, and A. Jablonski, "Cross sections for inner-shell ionization by electron impact," J. Phys. Chem. Ref. Data **43**(1), 013102 (2014).
[63]N. Ferreira, L. Sigaud, and E. C. Montenegro, "Three-body fragmentation from single ionization of water by electron impact: The role of satellite states," J. Phys. Chem. A **121**(17), 3234–3238 (2017).
[64]X. Liu and D. E. Shemansky, "Analysis of electron impact ionization properties of methane," J. Geophys. Res.: Space Phys. **111**(A4), A04303, https://doi.org/10.1029/2005JA011454 (2006).
[65]S. Xu, X. Ma, X. Ren, A. Senftleben, T. Pflüger, S. Yan, P. Zhang, J. Yang, J. Ullrich, and A. Dorn, "An (e, 2e + ion) investigation of dissociative ionization of methane," J. Chem. Phys. **138**(13), 134307 (2013).
[66]S. Pignataro, R. D. Marino, G. Distefano, and A. Mangini, "Core ionization energies and multi-peak structure of esca bands in some pentatomic heterocyclic compounds," Chem. Phys. Lett. **22**(2), 352–355 (1973).
[67]G. de Alti, P. Decleva, and A. Lisini, "An *ab initio* study of the satellite structure in the heteroatom core ionization of furan, pyrrole and thiophene," Chem. Phys. **90**(3), 231–242 (1984).
[68]S. A. Chambers and T. D. Thomas, "Satellite structure in the x-ray photoelectron spectra of gaseous furan, pyrrole, and thiophen," J. Chem. Phys. **67**(6), 2596–2603 (1977).
[69]M. Dampc, I. Linert, and M. Zubek, "Ionization and fragmentation of furan molecules by electron collisions," J. Phys. B: At., Mol. Opt. Phys. **48**(16), 165202 (2015).
[70]T. Kaneyasu, M. Ito, K. Soejima, Y. Hikosaka, and E. Shigemasa, "Site-specific formation of metastable OCS^{2+} studied by Auger-electron-ion coincidence method," J. Phys. B: At., Mol. Opt. Phys. **48**(12), 125101 (2015).
[71]N. Ferreira, L. Sigaud, and E. C. Montenegro, "Molecular fragmentation by electron impact investigated using a time delayed spectroscopic technique," J. Phys.: Conf. Ser. **488**(1), 012042 (2014).
[72]L. Sigaud, N. Ferreira, and E. C. Montenegro, "Absolute cross sections for O_2 dication production by electron impact," J. Chem. Phys. **139**(2), 024302 (2013).